

# Mind the memory: Artefactual scaling of energy dissipation rate due to inconsistent time reversal

Tassilo Schwarz,<sup>1,2</sup> Anatoly B. Kolomeisky,<sup>3,4</sup> and Aljaž Godec<sup>1,\*</sup>

<sup>1</sup>*Mathematical bioPhysics group, Max Planck Institute for Multidisciplinary Sciences, 37077 Göttingen, Germany*

<sup>2</sup>*Mathematical Institute, University of Oxford, Oxford, OX2 6GG, United Kingdom*

<sup>3</sup>*Department of Chemistry, Rice University, Houston, Texas 77005, USA*

<sup>4</sup>*Center for Theoretical Biological Physics, Department of Chemical and Biomolecular Engineering and Department of Physics and Astronomy, Rice University, Houston, Texas 77005, USA*

It has been recently proposed that an observed inverse power-law dependence of the Markovian estimate for the steady-state dissipation rate on the coarse-graining scale in self-similar networks reflects a scale-dependent energy dissipation. By explicit examples, it is demonstrated here that there are in general *no* relations between such an apparent power-law dependence and the actual dissipation on different length scales. We construct fractal networks with a single dissipative scale and networks with a true inverse energy-dissipation cascade, and show that they display the same scaling behavior. Moreover, it is shown that a self-similar network structure does *not* imply an inverse power-law scaling but may be mistaken for one in practice. When no dissipative cycles become hidden by the coarse graining, any scale dependence of the dissipation estimate vanishes if the memory is correctly accounted for in the time-reversal operation. A scale dependence of *higher-order* dissipation estimators signifies hidden dissipative cycles. Our results underscore the importance of accounting for memory effects in analyzing coarse observations.

Measurements in complex systems usually have finite resolution [1–4] or do *not* resolve at all relevant degrees of freedom—they just probe some low-dimensional projections of the dynamics, where many microscopic states become “lumped” onto the same observable “state”. Typical examples are macroscopic observables in condensed matter systems, such as magnetization [5], dielectric response [6], and diverse order parameters [7–9], as well as other observables (e.g. molecular extensions or FRET efficiencies and lifetimes) in single-molecule [10–19] and particle-tracking [20, 21] experiments.

It has been known that such coarse graining introduces memory in the dynamics of the observable quantities [22–24] (see [3] for the effect of a finite resolution). Much less is understood about the properties of out-of-equilibrium systems that display memory. In particular, a consistent formulation [25–33] and inference [33–38] of dissipation in the presence of slow dissipative hidden degrees of freedom is often a daunting task. It is very difficult to reliably infer violations of time reversibility (i.e., the detailed balance) from experiments on individual molecules [35, 39].

Violations of detailed balance on the level of individual stochastic trajectories  $\Gamma_t \equiv (x_\tau)_{0 \leq \tau \leq t}$  may be quantified via the steady-state dissipation (entropy production) rate  $\dot{S}$ . Given a *physically consistent* time-reversal operation  $\theta$ ,  $\dot{S}$  is defined as the relative entropy between the probability measure of a path  $P[\Gamma_t]$  and its time reverse  $P[\theta\Gamma_t]$  per unit time [40–42], i.e.

$$\dot{S}[\Gamma_t] = k_B \lim_{t \rightarrow \infty} \frac{1}{t} \left\langle \ln \frac{P[\Gamma_t]}{P[\theta\Gamma_t]} \right\rangle, \quad (1)$$

where  $\langle \cdot \rangle$  denotes the average over  $P[\Gamma_t]$  and  $k_B$  is Boltzmann’s constant. When  $x_t$  is an overdamped Markov

dynamics, we simply have  $\theta\Gamma_t = (x_{t-\tau})_{0 \leq \tau \leq t}$ . Specifically, for an ergodic Markov process on a discrete state space  $V$  with transition rates  $L_{ji}$  from state  $i$  to  $j$  and stationary probabilities  $P^s$ , Eq. (1) becomes [40–42]

$$\dot{S}_M[\Gamma_t] = k_B \sum_{i < j} (L_{ji}P_i^s - L_{ij}P_j^s) \ln \frac{L_{ji}}{L_{ij}}. \quad (2)$$

For thermodynamic consistency we must always have  $L_{ji} > 0 \implies L_{ij} > 0$  for any  $i, j \neq i \in V$  [42]. We henceforth express all estimates of  $\dot{S}$  in units of  $k_B$ .

When a coarse-grained version  $\hat{X}_t$  of the process is observed, where several microscopic states are lumped into the same observable state, provided a physically consistent time reversal  $\theta$  [25, 31, 37, 43], the definition in Eq. (1) with lumped paths  $\hat{\Gamma}_t = (\hat{X}_\tau)_{0 \leq \tau \leq t}$  still holds, whereas Eq. (2) does *not*. The reason is that  $\hat{X}_t$  displays memory (due to coarse-graining) which must be taken explicitly into account [31–33, 37, 44, 45]. If one simply replaces the rate  $L_{ji}$  between microscopic states in the Markovian result (2) with the effective rates between (mesoscopic) lumped states averaged over  $P^s$ , i.e. assuming (a potentially unphysical [32]) infinite timescale separation between dynamics within and between lumped states, one finds [27]  $\dot{S}_M[\hat{\Gamma}_t] \leq \dot{S}_M[\Gamma_t]$ . However, this inequality does *not* imply that a dependence of  $\dot{S}_M[\hat{\Gamma}_t]$  on the properties of the lumped state space carries any physical meaning since  $\dot{S}_M[\hat{\Gamma}_t]$  is *not* the dissipation rate of the coarse-grained process,  $\dot{S}_M[\hat{\Gamma}_t] \neq \dot{S}[\hat{\Gamma}_t]$ . Thermodynamic interpretations of  $\dot{S}_M[\hat{\Gamma}_t]$  (see, e.g. [46–49]) may lead to misconceptions, as we explicitly show below.

Energy dissipation is a critically important quantity since it measures how the system deviates from the equilibrium. It also sets the thermodynamic cost of biological functions [50, 51] and transport phenomena [52–59], such

\* agodec@mpinat.mpg.de

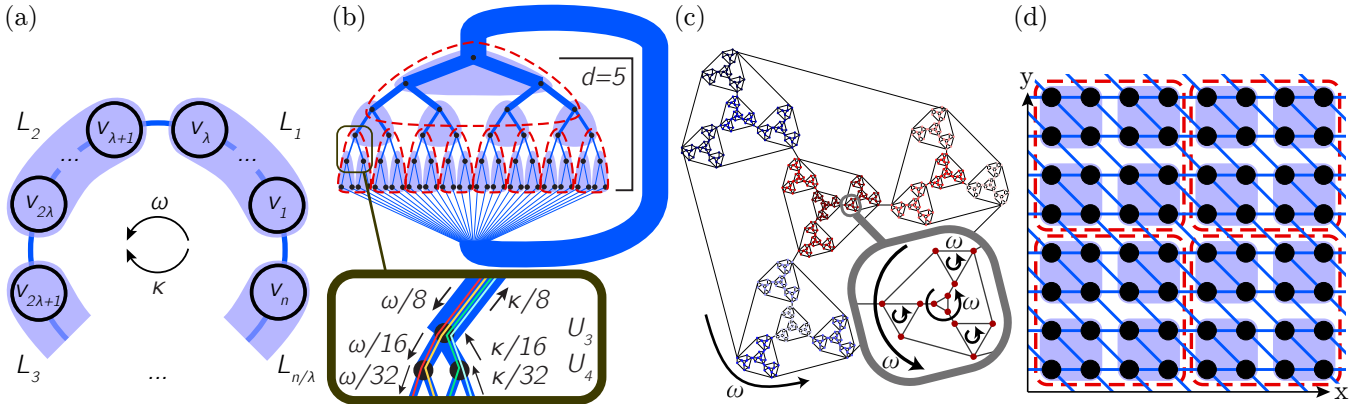


FIG. 1. Model systems: (a) Cycle graph with transition rates  $\omega$  and  $\kappa$  in counter-clockwise (+) and clockwise (-) direction, respectively. Lumps  $L_1, L_2, \dots, L_{n/\lambda}$  are highlighted in blue. (b) Tree of depth  $d = 5$  with lumps of depth  $l = 1$  (shaded in blue) and depth  $l = 2$  (circled in dashed red). Transition rates down + and up - (cyclic with respect to the thick edge) are set  $\propto \omega$  and  $\propto \kappa$ , respectively, chosen such that the cumulative transition rate between each level is  $\omega - \kappa$ . Self-similarity becomes obvious upon noticing that each tree consists of multiple smaller trees. Inset: Four fundamental cycles passing through the highlighted subgraph on levels  $U_3, U_4$  and corresponding transition rates. (c) Self-similar Sierpinski-type graph with lumps of size  $\lambda = 12$  indicated by the respective vertex coloring. A stationary current  $\omega$  runs through the outer side of each polygon, whereby the size of said polygons depends on the respective recursive depth. The depicted graph has recursion depth 5 and  $n = 768$  vertices. Inset: Element of recursion-depth 2 with all irreversible currents indicated by arrows. (d) Brusselator depicted as a grid graph as in [46]. A portion of the total  $n = 450 \times 450$  states is shown with lumps of size  $\lambda = 2 \times 2$  and  $\lambda = 4 \times 4$  shaded in blue and circled in dashed red, respectively.

as molecular-motor mediated transport of cargo [60, 61], coherent biochemical oscillations [62, 63], error correction in biochemical reactions [64–66], or cellular computations in sensing environmental cues [67]. These functions typically involve many processes coupled over multiple spatial and temporal scales [46, 50, 51]. It is thus of great interest to unravel how much energy is dissipated on different length scales.

To this end, recent works [46–48] investigated how the energy dissipation rate in self-similar non-equilibrium reaction networks depends on the coarse-graining scale  $\lambda \equiv n/n_s$  (i.e. the total number of microstates  $n$  relative to the number of mesoscopic states  $n_s$  in a lumped system) and observed a power-law dependence of the Markovian estimate  $\dot{S}_M[\hat{\Gamma}_t^s] \propto \lambda^{-\alpha}$  [46]. These findings were rationalized in terms of an “inverse cascade” of energy dissipation on different scales. In the specific context of active flows generated by the microtubule-kinesin motor system [68], this amounts to the claim that the most energy is spent to generate and maintain the flow at smaller length scales and only a tiny amount at large length scales [46]. While the underlying calculations in Refs. [46–48] are technically sound, their interpretation is physically inconsistent, as we show in this Letter.

Here we construct explicit examples invalidating such hypothesized implications between a power-law dependence of the Markovian dissipation estimates  $\dot{S}_M$  and the actual energy dissipated on different scales. In particular, we present fractal networks dissipating (i) only on a single (i.e., largest) length-scale and (ii) networks dissipating mostly on the smallest length scale and less on larger scales (i.e., networks with an “inverse energy dissipation

cascade” [46]) whereby both display the same scaling of  $\dot{S}_M$ . A self-similar network structure is shown to *not* even imply a power-law scaling of  $\dot{S}_M$ , suggesting that there is no relation between the power-law scaling of  $\dot{S}_M$  and the energy dissipated on a given scale. Moreover, the observed (apparent) power-law exponent changes upon progressively accounting for memory in the estimate for  $\dot{S}$ . The apparent power-law dependence of  $\dot{S}_M$  thus has *no* relation to the actual energy dissipated on a given scale and may simply be an artifact of an inconsistent time reversal. Extrapolations to the microscopic scale  $\lambda = 1$  are shown to be generally non-informative. Most importantly, when no dissipative cycles become hidden by the coarse graining, any scale dependence vanishes entirely once the memory is accounted for exactly when estimating  $\dot{S}$ . However, higher-order dissipation estimates are shown to be reliable indicators of the presence of hidden dissipative cycles. These observations emphasize the importance of properly accounting for memory effects in analyzing measurements from coarse observations.

*Setup.*—Let us consider continuous-time Markov processes  $x_t$  on a finite discrete state-space with  $L_{ji}$  denoting transition rates  $i \rightarrow j$ . We are interested in the steady-state dissipation rate  $\dot{S}$  in Eq. (1) in situations where one might only observe some coarse (i.e. lumped) version of the process that we denote as  $\hat{X}_t$ . For simplicity, and to align with the assumptions in [46], we assume the absence of kinetic hysteresis [31, 32, 37], i.e., that the coarse graining and time reversal commute. The observed process is hence a non-Markovian jump process on a partitioned “lumped space”, whereby the memory duration is finite but may become arbitrarily long depend-

ing on the coarse graining. In the following examples, the lumped process will correspond to a  $k$ -th order semi-Markov process with the instantaneous state  $\hat{X}_t$  depending on the previous  $k$  states. Thus,  $k = 1$  corresponds to a renewal process and, if the waiting time is exponentially distributed, to a Markov process. We will estimate  $\dot{S}[\hat{\Gamma}_t]$  within the simplest Markov approximation as in [46] as well as in terms of  $k$ -th order estimators [37] that account for memory. For simplicity and without any loss of we will neglect any potential waiting-time contributions (for further details see e.g. [37]). If we let  $\hat{\gamma}_k$  denote a particular set of  $k + 1$  consecutive observed states with  $k \geq 1$ , and  $P(\hat{\gamma}_k)$  the probability to observe this set along a (formally infinitely long) trajectory, then the  $k$ -th order estimator of  $\dot{S}$  is given by

$$\dot{S}_k^{\text{est}} \equiv \frac{1}{T_k} \sum_{\hat{\gamma}_k} P(\hat{\gamma}_k) \ln \frac{P(\hat{\gamma}_k)}{P(\theta\hat{\gamma}_k)} \leq \dot{S}, \quad (3)$$

where  $T_k$  is the average duration of a trajectory with  $k + 1$  observed states (i.e. with  $k$  observed state changes) and  $\theta\hat{\gamma}_k$  is the corresponding reversed set of  $k + 1$  states. If  $\hat{\Gamma}_t$  is a  $n$ -th order semi-Markov process then  $\dot{S}_{n+k}^{\text{est}} = \dot{S}_n^{\text{est}}$ ,  $\forall k > 0$ , and if  $\hat{\Gamma}_t = \Gamma_t$  is a Markov process we have  $\dot{S}_1^{\text{est}} = \dot{S}$ . Note, however, that when  $P(\hat{\gamma}_k)$  are inferred from trajectory data, undersampling may cause deviations from these relations.

*Example 1: Cycle graph.*—Consider Markovian dynamics on a (trivially self-similar) simple cycle with  $n \geq 4$  states with forward and backward transition rates  $\omega$  and  $\kappa \neq \omega$ , respectively (see Fig. 1a). The system has a single dissipative scale with an exact total dissipation rate

$$\dot{S} = (\omega - \kappa) \ln \left( \frac{\omega}{\kappa} \right). \quad (4)$$

As in [46], we decimate the state space in  $n/\lambda$  coarse-grained observable states (we assume  $n = 0 \pmod{\lambda}$ ), with “Markovian” forward and backward transition rates according to [46] given by  $\Omega(\lambda) = \omega/\lambda$  and  $K(\lambda) = \kappa/\lambda$ , respectively. We obtain a single dissipative cycle with homogeneous steady-state current  $J = (\lambda/n)[\Omega(\lambda) - K(\lambda)] = (\omega - \kappa)/n$  and affinity  $A = (n/\lambda) \ln(\omega/\kappa)$ , yielding the Markov estimate

$$\dot{S}_M = JA = \frac{1}{\lambda} (\omega - \kappa) \ln \left( \frac{\omega}{\kappa} \right) \propto \lambda^{-1}, \quad (5)$$

indeed an inverse power law according to [46]. However, the microscopic system has a single dissipative scale, the entire cycle. Thus, the scaling has *no* implications for the energy dissipation on distinct length scales. In fact, we now show that it is merely an artifact of inconsistent time reversal in the presence of memory.

The coarse process is non-Markovian, to be precise, it is a 2<sup>nd</sup>-order semi-Markov process (see also [32]). This means that the waiting time within, and probability for a forward/backward transition from, a lump depends on the previous state. The exact entropy production may be

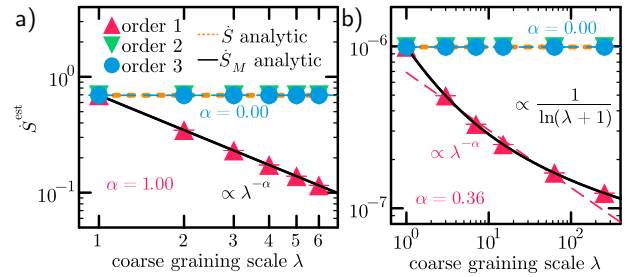


FIG. 2. Entropy-production estimates for different coarse-graining scales: (a)  $\dot{S}_k^{\text{est}}$  for the ring graph with  $n = 60$  states. Higher-order estimators ( $k \geq 2$ ) allows for correct inference of  $\dot{S}$  (green, blue), while omitting memory leads to an artefactual power law (black and red lines). Analytical results are fully corroborated by simulations. (b)  $\dot{S}_k^{\text{est}}$  for the tree of depth  $d = 23$ , i.e.  $n = 16777215$ . Higher-order estimators allow for correct inference of  $\dot{S}$  (green, blue), whereas ignoring memory leads to a spurious inverse energy cascade (black line), which may be easily mistaken for a power law (red dashed fit). In both cases, we considered 100 independent stationary trajectories each visiting  $10^9$  microscopic states.

determined via the two-step affinity  $A_2$  [32, 37, 44]

$$\dot{S}_2^{\text{est}} = JA_2 = J \ln \left( \frac{\Phi_{+|+}}{\Phi_{-|-}} \right) = \dot{S}, \quad (6)$$

where  $\Phi_{\pm|\pm}$  denotes the conditional stationary probability for a step in the  $\pm$  direction given that the previous step was also in the  $\pm$  direction, and the proof of the last equality is given in the Supplemental Material (SM). These results are verified via simulations in Fig. 2a. Equality, as opposed to a lower bound, emerges because no dissipative cycles become hidden, and the waiting-time contribution vanishes (see SM). Consistent time reversal and hence thermodynamics thus remove the artefactual scaling behavior.

*Example 2: Tree graph.*—We now consider a perfectly self-similar network with a single dissipative *scale* (i.e. the system size) but multiple (equivalent) dissipative *cycles* each with a stationary current  $J_c$  (see Fig. 1b). In this binary tree of depth  $d$ , every edge is bidirectional with rate  $\propto \omega$  in the “down” (+) and  $\propto \kappa$  in the “up” (−) direction, respectively, such that the cumulative transition rate between each level is  $\omega - \kappa$ . This way, the rates along adjacent edges in consecutive levels in both directions  $\pm$  are halved (see Inset in 1b). The detailed mathematical construction is described in Appendix A. The exact entropy production of the system in the cycle basis  $\mathcal{C}$  with  $2^d$  basis cycles reads (see proof in SM)

$$\dot{S} = \sum_{c \in \mathcal{C}} J_c A_c = \frac{d+1}{2^{d+1}-1} (\omega - \kappa) \ln \left( \frac{\omega}{\kappa} \right), \quad (7)$$

where the basis-cycle current (see [69] for details on cycle bases) is  $J_c = (\omega - \kappa)/2^d(2^{d+1} - 1)$ .

We lump the tree into mesoscopic states each having a depth  $l < d$  (see Fig. 1b). The Markovian estimate  $\dot{S}_M$

for such a lumped system reads (see derivation in SM)

$$\dot{S}_M = \frac{d+1}{2^{d+1}-1} \frac{\ln(2)}{\ln(\lambda+1)} (\omega - \kappa) \ln\left(\frac{\omega}{\kappa}\right) \propto \frac{1}{\ln(\lambda+1)}, \quad (8)$$

where  $\lambda = n/n_s = 2^{l+1} - 1$ . Now there is in fact strictly *no* power-law scaling of  $\dot{S}_M$  in  $\lambda$  despite a perfectly self-similar network structure. However, one may in practice identify a power-law  $\sim \lambda^{-0.36}$  (see Fig. 2b) as in [46]. Meanwhile, the microscopic system has a single dissipative scale, the system size. An observed power-law thus has *no* relation with energy dissipation on distinct scales and may *not* even be a power law. It is an artifact of inconsistent time reversal in the presence of memory.

The lumping yields a 2<sup>nd</sup>-order semi-Markov process and hides *no* dissipative cycles. By accounting for memory via  $\dot{S}_{k \geq 2}^{\text{est}}$  [32, 37, 44] we, therefore, recover the exact microscopic result (see derivation in SM)

$$\dot{S}_2^{\text{est}} = \frac{\omega - \kappa}{2^{d+1} - 1} \frac{d+1}{l+1} \ln\left(\frac{\Phi_{++}}{\Phi_{--}}\right) = \dot{S}_{k > 2}^{\text{est}} = \dot{S}, \quad (9)$$

where  $\Phi_{\pm|\pm}$  is the conditional probability for a transition between two lumps (at given coarseness) in the  $\pm$  direction given that the preceding step occurred in the  $\pm$  direction. According to the last equality, consistent time reversal (and hence correct thermodynamics) removes the artefactual scaling behavior. The analytical results are confirmed by simulations (Fig. 2b) and generalized to the more complex tree-diamond graph in Appendix C.

*Example 3: Sierpinski-type graph.*—As our next example, we consider a self-similar graph composed of nested polygons in the spirit of the Sierpinski fractal (see Fig. 1c). The rates are set such that each nested polygon is driven with  $\omega$ . Hence a polygon with recursive depth  $l$  has affinity  $A_l = 3l \ln \omega$  (see derivation in SM). The depth  $l = 1$  corresponds to innermost triangles. The detailed construction is described in SM. In contrast to the previous examples, this network is designed to indeed display a scale-dependent energy dissipation rate  $\dot{S}$ , whereby most energy is dissipated on the smallest and less energy on larger scales (for quantitative statements see SM). For networks with a recursive depth larger than 3, we are not able to determine  $P_i^s$  (and hence  $\dot{S}$ ) analytically and therefore resort to numerical methods to compute  $\dot{S}$  (see SM for details). In our analysis, we focus on a network with recursive depth 7 with 12288 microscopic states. The system was coarse-grained into lumps with recursive depth  $l$ , such that the lumped graph perfectly preserves the original fractal structure (see Fig. 1c). However, in stark contrast to the previous examples, the coarse graining here hides dissipative cycles. We determine  $\dot{S}_M$  via Eqs. (2-3) (with  $k = 1$ ) and  $\dot{S}_{k \geq 2}^{\text{est}}$  using Eq. (3) from 108 simulated steady-state trajectories each with a total duration  $5 \times 10^8$  steps.

Despite having properties that are “orthogonal” to the previous examples—featuring a scale-dependent energy dissipation rate and dissipative cycles becoming hidden

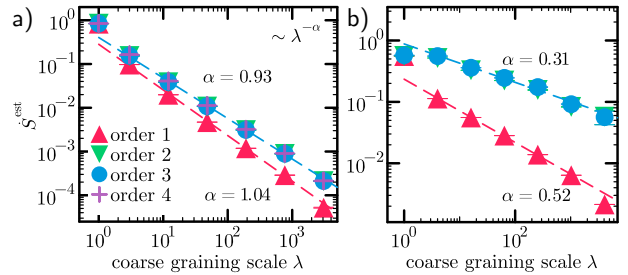


FIG. 3. Entropy-production estimates for different coarse-graining scales: (a)  $\dot{S}_2^{\text{est}}$  for Sierpinski-type graph for recursion depth 7 ( $n = 12288$  vertices). We find  $\dot{S}_M \propto \lambda^{-1}$  while higher-order estimators  $\dot{S}_{k \geq 2}^{\text{est}}$  converge to a power law with  $\alpha = 0.93$ , hinting at a 2<sup>nd</sup> (or perhaps 3<sup>rd</sup>) order semi-Markov process. (b)  $\dot{S}_2^{\text{est}}$  for the Brusselator with  $n = 202500$  vertices. The virtual power law for the Markov estimate  $\dot{S}_1^{\text{est}} \propto \lambda^{-0.52}$  is faster decaying  $\dot{S}_{k \geq 2}^{\text{est}} \propto \lambda^{-0.31}$  obtained by accounting for memory. For simulation details see SM.

by the lumping—it *resembles* the same power-law scaling of the Markovian estimate  $\dot{S}_M \propto \lambda^{-\alpha}$  (red line Fig. 3a) in fact with the same exponent  $\alpha \approx 1$  as in Eq. (5). This shows once more that a power-law scaling of  $\dot{S}_M$ , and in particular also the exponent, does *not* give any indication about dissipation on different lengths scales. Moreover, the exponent  $\alpha$  changes to  $\approx 0.9$  upon accounting for memory via  $\dot{S}_{k \geq 2}^{\text{est}}$  (blue line Fig. 3a), and it appears that the lumping yields a 2<sup>nd</sup> (or perhaps 3<sup>rd</sup>) order semi-Markov process, since  $\dot{S}_{2,3}^{\text{est}} = \dot{S}_4^{\text{est}}$ . The fact that  $\dot{S}_{k \geq 2}^{\text{est}} < \dot{S}$  (i.e. equality not reached) is because dissipative cycles are hidden by the coarse graining.

*Example 4: Brusselator.*—Finally, let us consider the Brusselator model [70–72] (see Fig. 1d) as in [46], here with 202500 microscopic states. We perform the coarse graining as was done in [46], two levels of coarse graining are highlighted in Fig. 1d. We estimate  $\dot{S}$ ,  $\dot{S}_M$ , and  $\dot{S}_{k \geq 2}^{\text{est}}$  from 25 simulated stationary trajectories each having  $10^9$  steps (skipping  $10^9$  initial steps). Using Eq. (3) with  $k = 1$  we infer  $\dot{S}_M$  that agrees with the results in [46] (red triangles in Fig. 3b). In particular, we reproduce the apparent power-law scaling  $\dot{S}_M \propto \lambda^{-\alpha}$  with the same exponent as in [46], i.e.  $\alpha \approx 0.52$ . Coincidentally, it is of the same order as the *virtual* power-law of the tree and tree-diamond with  $\alpha \approx 0.3$  (see Appendix C), which in reality is *not* a power law at all (see Eq. (8)).

We now account for memory in the time-reversal via  $\dot{S}_{k \geq 2}^{\text{est}}$ . The lumped process is apparently 2<sup>nd</sup> or 3<sup>rd</sup> order semi-Markov as  $\dot{S}_{2,3}^{\text{est}} = \dot{S}_4^{\text{est}}$ . The fact that  $\dot{S}_{k \geq 2}^{\text{est}} < \dot{S}$  is a consequence of dissipative cycles that become hidden by the coarse graining. Higher-order estimates also display an apparent power-law scaling albeit with a smaller exponent  $\dot{S}_{k \geq 2}^{\text{est}} \propto \lambda^{-0.31}$  for considered  $\omega, \kappa$ . However, according to previous counterexamples, we must conclude that these power laws in fact have *no* implications about energy dissipation on different length scales.

*Interpreting scalings under consistent time reversal.*—An apparent power-law dependence of  $\dot{S}_M$  on the coarse-graining scale  $\lambda$  generally has *no* relation with the microscopic dissipation mechanisms. However, meaningful information about the underlying dynamics may still be inferred from coarse-grained data under consistent time reversal. More specifically, if we can find an order  $n$  such that  $\dot{S}_{n+k}^{\text{est}} = \dot{S}_n^{\text{est}}$  for any  $k \geq 1$ . If for such  $n, k$  we find that  $\dot{S}_{n+k}^{\text{est}} \propto \lambda^{-\alpha}$  for some  $\alpha > 0$ , one *concludes* that the coarse graining hides dissipative cycles (this is *not* true for a scaling of  $\dot{S}_M$ ). If (and only if) in addition, we have information supporting a self-similar network structure, we may also assume that most energy is dissipated on the smallest and less energy on larger scales.

It is important to emphasize that generally *no* such conclusion can be drawn if we observe a coarse-graining scale independence, i.e.  $\dot{S}_{n+k}^{\text{est}} \propto \lambda^0$  for  $\lambda > 1$ . Only if we observe independence extending to  $\lambda = 1$  we may conclude that no dissipative cycles become hidden by the coarse graining. Extrapolations  $\lambda \rightarrow 1$  generally yield erroneous conclusions about the microscopic dissipation time scales (for a detailed discussion, see Appendix B).

*Conclusion.*—Several explicit examples that invalidate the recently proposed relation between an apparent power-law dependence of Markovian estimates for the energy dissipation rate  $\dot{S}_M$  from coarse-grained observations and the actual dissipation on different length scales were presented and analyzed. We constructed fractal networks with a single dissipative scale and self-similar networks with an “inverse energy dissipation cascade” [46], where most energy is dissipated on the smallest and less energy on larger scales. Both systems exhibit the same scaling behavior of the energy dissipation at different scales. The apparent scaling exponent gradually reduces upon accounting for memory in the dissipation estimates. When no dissipative cycles become hidden by the coarse graining, any scale dependence vanishes as soon as the memory is accounted for exactly in the time-reversal operation and we can infer the microscopic dissipation. Therefore, an inverse power-law dependence of the dissipation rate generally has *no* implications for scale-dependent energy dissipation and may simply be an artifact of inconsistent time reversal in the presence of memory. However, it may still be possible to infer meaningful information about the microscopic dynamics, e.g. the presence of hidden dissipative cycles, via higher-order dissipation estimators which incorporate a consistent time reversal in the presence of memory. This further highlights the importance and benefits of accounting for memory in analyzing data from coarse observations.

*Acknowledgments.*—Financial support from the European Research Council (ERC) under the European Union’s Horizon Europe research and innovation program (Grant Agreement No. 101086182 to A. G.) and from the Studienstiftung des Deutschen Volkes and the Rhodes Trust (to T. S.) are acknowledged. ABK also acknowledges the support from the Welch Foundation (Grant C-1559) and the Center for Theoretical Biological Physics

sponsored by the NSF (PHY-2019745).

*Appendix A: Construction of tree graph.*—Consider a tree graph of depth  $d$ , i.e., vertices are on levels  $U_0, \dots, U_d$ , where level  $i$  contains  $|U_i| = 2^i$  vertices. For  $i < d$ , each vertex  $v \in U_i$  has two offsprings  $x, y \in U_{i+1}$  with rates  $L_{xv} = L_{yv} = \omega/2^{i+1}$  in + direction and  $L_{vx} = L_{vy} = \kappa/2^{i+1}$  in - direction. Vertices in the bottom level  $v \in U_d$  have edges of rate  $\omega/2^d$  towards the root, and rate  $\kappa/2^d$  from the root to each  $v$ .

*Appendix B: Problematic extrapolation to microscopic scales.*—Assuming that the power-law scaling of dissipation rate truly reflects dissipation on distinct length scales, one may attempt to extrapolate  $\dot{S}_M \propto \lambda^{-\alpha}$  and  $\dot{S}_{k \geq 2}^{\text{est}} \propto \lambda^{-\alpha}$  to microscopic scales, that is, to vanishing coarse graining  $\lambda \rightarrow 1$  (see [46]). In the case of the cycle-graph which has a single (i.e. macroscopic) dissipative length scale this would coincidentally (and conceptually somewhat paradoxically) yield the exact microscopic result (compare Eqs. (4) and (5) in the limit  $\lambda \rightarrow 1$ ). In all other examples, extrapolating  $\dot{S}_M$  to  $\lambda = 1$  would yield a lower bound. This may be useful for bounding  $\dot{S}$  from below (the bound  $\dot{S}_M \leq \dot{S}$  was obtained in [27]). However, there are strictly self-similar networks (e.g. the tree and tree-diamond graph) which do *not* display a power-law scaling of energy dissipation rate but where one may nevertheless (erroneously) identify a power law. It is conceivable that such examples may lead to an overestimation of  $\dot{S}$ . Extrapolated values should thus be interpreted with great care, especially when the underlying microscopic topology of the network is not known. Similarly, our examples in Fig. 3 show that one must also *not* extrapolate apparent power-law scalings of higher-order estimates  $\dot{S}_{k \geq 2}^{\text{est}}$  as these may lead to overestimating  $\dot{S}$ .

*Appendix C: Tree diamond graph.*—We now consider a non-trivially self-similar network with a single dissipative scale (i.e., the system size) but multiple (equivalent) dissipative cycles each with a stationary current  $J_c$  (see Fig. 4a). It corresponds to a “tree diamond” obtained by merging two binary trees of depth  $d$  such that they have the same set of leaves. Every edge is bidirectional with a rate  $\propto \omega$  in + and  $\propto \kappa$  in - direction, respectively, such that the cumulative transition rate between each level is  $\omega - \kappa$ . This way, the edge entering the root in + direction has rate  $\omega$ , while the rates along the remaining edges are split evenly amongst the branches, (see Fig. 4a). The detailed mathematical construction is described in the SM. The exact entropy production of the system in the cycle basis  $\mathcal{C}$  with  $2^d$  basis cycles reads (see proof in SM)

$$\dot{S} = \sum_{c \in \mathcal{C}} J_c A_c = \frac{2d+1}{n(d)} (\omega - \kappa) \ln \left( \frac{\omega}{\kappa} \right). \quad (10)$$

where  $n(d) = 2^{d+1} - 1 + 2^d - 1 = 3 \cdot 2^d - 2$  is the number of states in a diamond with depth  $d$ , and the basis-cycle current (see [69]) reads  $J_c = (\omega - \kappa)/n(d)2^d$ .

We lump the network into lumps of depth  $l < d$ , whereby the  $2^{d-l}$  distinct lumps on the “equator” are treated separately (see Fig. 4b). The Markovian estimate

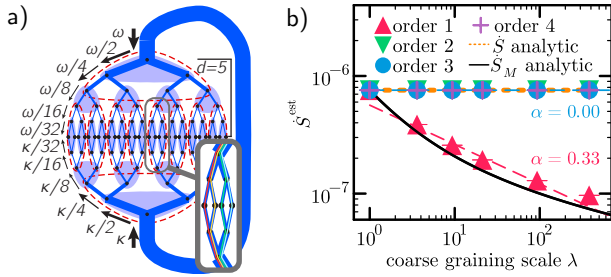


FIG. 4. (a) Tree diamond graph of depth  $d = 5$  with lumps of depth  $l = 1$  (shaded in blue) and depth  $l = 2$  (circled in dashed red). Transition rates in down (+) and up (-) direction (cyclic with respect to the thick blue edge) are taken to be  $\propto \omega$  and  $\propto \kappa$ , respectively, chosen such that the cumulative transition rates between each level is  $\omega - \kappa$ . The self-similarity becomes obvious upon noticing that each tree diamond consists of multiple smaller tree diamonds. Inset: Four fundamental cycles pass through the highlighted subgraph of depth  $d = 2$ . (b) Entropy-production estimates for different coarse-graining scales; Estimators  $\dot{S}_k^{\text{est}}$  provide an exact estimation of  $\dot{S}$  for higher orders ( $k \geq 2$ ), matching the analytical prediction (yellow line). Ignoring memory leads to a *virtual* energy dissipation cascade, which has *no* implications for dissipation on different scales. The virtual cascade is actually *not* even a power law, but may be mistaken for one.

of such a lumped system is given by (see SM)

$$\dot{S}_M = \frac{\omega - \kappa}{n(d)} \frac{2d - l + 1}{l + 1} \ln\left(\frac{\omega}{\kappa}\right) \stackrel{d \gg l \gg 1}{\propto} \frac{1}{l} \propto \frac{1}{\ln(\lambda/3)}, \quad (11)$$

where  $\lambda = n/n_s$  now corresponds, by definition, to the average lump size. As in the tree graph, there is in fact strictly *no* power-law scaling of  $\dot{S}_M$  in  $\lambda$  despite a perfectly self-similar network structure. Moreover, as shown in Fig. 4b, one may in practice easily identify a power-law  $\sim \lambda^{-0.33}$  in agreement with [46]. As in the tree graph, the microscopic system has a single dissipative scale, further underscoring that an observed power law has *no* implications for energy dissipation on distinct scales and may *not* even be a power law. It is an artifact of inconsistent time reversal in the presence of memory.

The lumping yields a 2<sup>nd</sup>-order semi-Markov process and no dissipative cycles become hidden. By accounting for memory via  $\dot{S}_{k \geq 2}^{\text{est}}$  we recover the microscopic result (see derivation in SM)

$$\dot{S}_2^{\text{est}} = \frac{\omega - \kappa}{n(d)} \left[ 2 \frac{d-l}{l+1} \ln\left(\frac{\Phi_{+|+}^{\Delta}}{\Phi_{-|-}^{\Delta}}\right) + \ln\left(\frac{\Phi_{+|+}^{\diamond}}{\Phi_{-|-}^{\diamond}}\right) \right] = \dot{S}, \quad (12)$$

where  $\Phi_{\pm|\pm}^{\Delta}$  is the conditional probability for a transition between two lumps (at given coarseness) in the  $\pm$  direction given that the preceding step occurred in the  $\pm$  direction in the top and bottom part of the network (the factor of two is due to symmetry), and  $\Phi_{\pm|\pm}^{\diamond}$  the corresponding conditional probability for a transition in the  $\pm$  direction in any of the equatorial lumps. By the last equality consistent time reversal (and thus thermodynamics) removes the artefactual scaling behavior.

- 
- [1] J. Gladrow, N. Fakhri, F. C. MacKintosh, C. F. Schmidt, and C. P. Broedersz, *Phys. Rev. Lett.* **116**, 248301 (2016).
- [2] C. Battle, C. P. Broedersz, N. Fakhri, V. F. Geyer, J. Howard, C. F. Schmidt, and F. C. MacKintosh, *Science* **352**, 604–607 (2016).
- [3] C. Dieball and A. Godec, *Phys. Rev. Lett.* **129**, 140601 (2022).
- [4] C. Dieball and A. Godec, *Phys. Rev. Res.* **4**, 033243 (2022).
- [5] D. Hérisson and M. Ocio, *Phys. Rev. Lett.* **88**, 257202 (2002).
- [6] H. Oukris and N. E. Israeloff, *Nat. Phys.* **6**, 135–138 (2009).
- [7] A. J. Bray, S. N. Majumdar, and G. Schehr, *Adv. Phys.* **62**, 225–361 (2013).
- [8] S. Burov, R. Metzler, and E. Barkai, *Proc. Natl. Acad. Sci.* **107**, 13228–13233 (2010).
- [9] J. H. P. Schulz, E. Barkai, and R. Metzler, *Phys. Rev. X* **4**, 011028 (2014).
- [10] A. K. Sangha and T. Keyes, *J. Phys. Chem. B* **113**, 15886–15894 (2009).
- [11] S. S. Plotkin and P. G. Wolynes, *Phys. Rev. Lett.* **80**, 5015 (1998).
- [12] W. Min, G. Luo, B. J. Cherayil, S. C. Kou, and X. S. Xie, *Phys. Rev. Lett.* **94**, 198302 (2005).
- [13] D. E. Makarov, *J. Chem. Phys.* **138** (2013), 10.1063/1.4773283.
- [14] J. Brujić, R. I. Hermans Z., K. A. Walther, and J. M. Fernandez, *Nat. Phys.* **2**, 282–286 (2006).
- [15] I. Grossman-Haham, G. Rosenblum, T. Namani, and H. Hofmann, *Proc. Natl. Acad. Sci.* **115**, 513–518 (2018).
- [16] I. M. Sokolov, *Phys. Rev. Lett.* **90**, 080601 (2003).
- [17] T. Guérin, O. Bénichou, and R. Voituriez, *Nat. Chem.* **4**, 568–573 (2012).
- [18] A. M. Berezhkovskii and D. E. Makarov, *J. Phys. Chem. Lett.* **9**, 2190–2195 (2018).
- [19] A. Lapolla and A. Godec, *Phys. Rev. Res.* **3**, L022018 (2021).
- [20] F. Ginot, J. Caspers, M. Krüger, and C. Bechinger, *Phys. Rev. Lett.* **128**, 028001 (2022).
- [21] N. Narinder, C. Bechinger, and J. R. Gomez-Solano, *Phys. Rev. Lett.* **121**, 078003 (2018).

- [22] S. Nordholm and R. Zwanzig, *Journal of Statistical Physics* **13**, 347–371 (1975).
- [23] H. Grabert, P. Talkner, P. Hänggi, and H. Thomas, *Z. Phys. B: Cond. Matt.* **29**, 273–280 (1978).
- [24] M. Ferrario and P. Grigolini, *J. Math. Phys.* **20**, 2567 (2008).
- [25] H. Wang and H. Qian, *J. Math. Phys.* **48**, 013303 (2007).
- [26] J. Mehl, B. Lander, C. Bechinger, V. Blickle, and U. Seifert, *Phys. Rev. Lett.* **108**, 220601 (2012).
- [27] M. Esposito, *Phys. Rev. E* **85**, 041125 (2012).
- [28] A. Puglisi, S. Pigolotti, L. Rondoni, and A. Vulpiani, *J. Stat. Mech.* **2010**, P05015 (2010).
- [29] G. Teza and A. L. Stella, *Phys. Rev. Lett.* **125**, 110601 (2020).
- [30] P. Talkner and P. Hänggi, *Rev. Mod. Phys.* **92**, 041002 (2020).
- [31] D. Hartich and A. Godec, *Phys. Rev. X* **11**, 041047 (2021).
- [32] D. Hartich and A. Godec, *Phys. Rev. Res.* **5**, L032017 (2023).
- [33] J. van der Meer, B. Ertel, and U. Seifert, *Phys. Rev. X* **12**, 031025 (2022).
- [34] P. E. Harunari, A. Dutta, M. Polettini, and E. Roldán, *Phys. Rev. X* **12**, 041026 (2022).
- [35] A. Godec and D. E. Makarov, *J. Phys. Chem. Lett.* **14**, 49–56 (2022).
- [36] J. van der Meer, J. Degünther, and U. Seifert, *Phys. Rev. Lett.* **130**, 257101 (2023).
- [37] K. Blom, K. Song, E. Vouga, A. Godec, and D. E. Makarov, *Proc. Natl. Acad. Sci.* **121** (2024), 10.1073/pnas.2318333121.
- [38] J. Degünther, J. van der Meer, and U. Seifert, *Proc. Natl. Acad. Sci.* **121** (2024), 10.1073/pnas.2405371121.
- [39] C. Ratzke, B. Hellenkamp, and T. Hugel, *Nat. Commun.* **5**, 4192 (2014).
- [40] J. L. Lebowitz and H. Spohn, *J. Stat. Phys.* **95**, 333–365 (1999).
- [41] P. Gaspard, *J. Chem. Phys.* **120**, 8898–8905 (2004).
- [42] U. Seifert, *Rep. Prog. Phys.* **75**, 126001 (2012).
- [43] D. Hartich and A. Godec, *Nat. Commun.* **15** (2024), 10.1038/s41467-024-52602-0.
- [44] I. A. Martínez, G. Bisker, J. M. Horowitz, and J. M. R. Parrondo, *Nat Commun* **10**, 3542 (2019).
- [45] X. Zhao, D. Hartich, and A. Godec, *Phys. Rev. Lett.* **132**, 147101 (2024).
- [46] Q. Yu, D. Zhang, and Y. Tu, *Phys. Rev. Lett.* **126**, 080601 (2021).
- [47] L. Cocconi, G. Salbreux, and G. Pruessner, *Phys. Rev. E* **105**, L042601 (2022).
- [48] Q. Yu and Y. Tu, *Phys. Rev. E* **105**, 044140 (2022).
- [49] Q. Yu and P. E. Harunari, “Dissipation at limited resolutions: Power law and detection of hidden dissipative scales,” (2024), arXiv:2407.13707.
- [50] H. Qian, *Annu. Rev. Phys. Chem.* **58**, 113–142 (2007).
- [51] R. D. Astumian, *Annu. Rev. Biophys.* **40**, 289–313 (2011).
- [52] N. Shiraishi, K. Funo, and K. Saito, *Phys. Rev. Lett.* **121**, 070601 (2018).
- [53] E. Aurell, C. Mejía-Monasterio, and P. Muratore-Ginanneschi, *Phys. Rev. Lett.* **106**, 250601 (2011).
- [54] S. Ito and A. Dechant, *Phys. Rev. X* **10**, 021056 (2020).
- [55] N. Shiraishi and K. Saito, *Phys. Rev. Lett.* **123**, 110603 (2019).
- [56] G. Falasco and M. Esposito, *Phys. Rev. Lett.* **125**, 120604 (2020).
- [57] S. Ito and A. Dechant, *Phys. Rev. X* **10**, 021056 (2020).
- [58] T. Van Vu and K. Saito, *Phys. Rev. X* **13**, 011013 (2023).
- [59] C. Dieball and A. Godec, *Phys. Rev. Lett.* **133**, 067101 (2024).
- [60] A. B. Kolomeisky and M. E. Fisher, *Annu. Rev. Phys. Chem.* **58**, 675–695 (2007).
- [61] U. Seifert, *Phys. Rev. Lett.* **106**, 020601 (2011).
- [62] L. Oberreiter, U. Seifert, and A. C. Barato, *Phys. Rev. E* **106**, 014106 (2022).
- [63] Y. Cao, H. Wang, Q. Ouyang, and Y. Tu, *Nat. Phys.* **11**, 772–778 (2015).
- [64] J. J. Hopfield, *Proc. Natl. Acad. Sci.* **71**, 4135–4139 (1974).
- [65] J. Ninio, *Biochimie* **57**, 587 (1975).
- [66] J. D. Mallory, O. A. Igoshin, and A. B. Kolomeisky, *J. Phys. Chem. B* **124**, 9289 (2020).
- [67] P. Mehta and D. J. Schwab, *Proc. Natl. Acad. Sci.* **109**, 17978–17982 (2012).
- [68] T. Sanchez, D. T. N. Chen, S. J. DeCamp, M. Heymann, and Z. Dogic, *Nature* **491**, 431–434 (2012).
- [69] J. Schnakenberg, *Rev. Mod. Phys.* **48**, 571 (1976).
- [70] G. Nicolis and I. Prigogine, *Self-Organization in Nonequilibrium Systems*, 1st ed. (Wiley, New York, 1977).
- [71] H. Qian, S. Saffarian, and E. L. Elson, *Proc. Natl. Acad. Sci.* **99**, 10376–10381 (2002).
- [72] J. H. Fritz, B. Nguyen, and U. Seifert, *J. Chem. Phys.* **152** (2020), 10.1063/5.0006115.
- [4] Even stronger, inverting the matrix from Eq. (S42) yields the same denominator for each entry, hence we get the same roots, and hence the same powers of the exponentials in the waiting time distribution.
- [5] The last level in the upper half of the macroscopic tree diamond that roots a tree lump is level  $d - 2l - 1$ .

**Supplemental Material for:**

**Mind the memory: Artefactual scaling of energy dissipation rate due to inconsistent time reversal**

Tassilo Schwarz<sup>1,2</sup>, Anatoly B. Kolomeisky<sup>3,4</sup>, and Aljaž Godec<sup>1</sup>

<sup>1</sup>*Mathematical bioPhysics Group, Max Planck Institute for Multidisciplinary Sciences, 37077 Göttingen, Germany*

<sup>2</sup>*Mathematical Institute, University of Oxford, Oxford, OX2 6GG, United Kingdom*

<sup>3</sup>*Department of Chemistry, Rice University, Houston, Texas 77005, USA*

<sup>4</sup>*Center for Theoretical Biological Physics, Department of Chemical and Biomolecular Engineering and Department of Physics and Astronomy, Rice University, Houston, Texas 77005, USA*

In this Supplemental Material we provide further details on the models, the underlying calculations, and some further technicalities. In addition, we give details on the model parameters and numerical considerations.

**CONTENTS**

I.	Notation	2
II.	Splitting probabilities in lumped cycle graph $C_n$	2
	A. Note on the waiting time distribution	2
III.	Tree graph	4
	A. Microscopic dynamics	4
	B. Mistaken dynamics	4
	C. Mesosystem	5
IV.	Sierpinski-type graph	5
	A. Decomposition in cycle basis	5
	B. Comparison of stochastic estimator to analytic solution	5
V.	Brusselator	6
VI.	Tree diamond graph	7
	A. Construction	8
	B. Microscopic dynamics	8
	1. $\dot{S}$ via edges	8
	2. Cycle decomposition	8
	C. Mesosystem	9
	1. Splitting probability $\Phi$ for tree lump	9
	2. Splitting probability $\Phi$ for tree diamond lump	11
	D. Average lump size	12
	E. Mistaken dynamics	12
VII.	Technicalities of the sampling procedure	13
	A. Exploiting the symmetry of the graph	13
	B. Choice of parameters	13
	C. Subsampling for higher orders	14
	References	14



## I. NOTATION

Throughout we use the following conventions:

- For  $n \in \mathbb{N}$ , we define  $[n] \equiv \{1, \dots, n\}$ .
- $L$  corresponds to the generator of the considered underlying/microscopic Markov process.

## II. SPLITTING PROBABILITIES IN LUMPED CYCLE GRAPH $C_n$

In this section, we determine the splitting probabilities in the lumped cycle graph via the Laplace transform. Consider the graph depicted in Fig. 1a in the Letter, that is, a cycle graph  $C_n$  of  $n$  states and with  $n/\lambda \in \mathbb{N}$  many lumps of size  $\lambda \in \mathbb{N}$ . We focus, without loss of generality (w.l.o.g.), on the first lump. For state  $i \in [\lambda]$ , we have the following system of  $\lambda$  coupled differential equations

$$\frac{dp_i}{dt} = -(\omega + \kappa)p_i + \mathbb{1}_{i>1}\omega p_{i-1} + \mathbb{1}_{i<n}\kappa p_{i+1}, \quad (\text{S1})$$

with absorbing boundaries

$$\frac{dp_{\lambda+1}}{dt} = \omega p_\lambda, \quad \frac{dp_n}{dt} = \kappa p_1. \quad (\text{S2})$$

In Laplace space ( $\tilde{p}(s) \equiv \int_0^\infty p(t) \exp(-st) dt$ ), we obtain

$$\begin{pmatrix} s + \omega + \kappa & -\kappa & & & & \\ -\omega & s + \omega + \kappa & -\kappa & & & \\ & & \ddots & \ddots & \ddots & \\ & & & -\omega & s + \omega + \kappa & -\kappa \\ & & & -\omega & s + \omega + \kappa & \end{pmatrix} \begin{pmatrix} \tilde{p}_1(s) \\ \tilde{p}_2(s) \\ \vdots \\ \vdots \\ \tilde{p}_\lambda(s) \end{pmatrix} = \begin{pmatrix} p_1(0) \\ p_2(0) \\ \vdots \\ \vdots \\ p_\lambda(0) \end{pmatrix}. \quad (\text{S3})$$

Denoting the tridiagonal matrix in Eq. (S3) by  $M(s)$  and by  $p_{j|i}(t)$  the probability of having reached state  $j$  by time  $t$  given that we started in state  $i$ , we have for the ratio of splitting probabilities

$$\begin{aligned} \frac{\Phi_{+|+}}{\Phi_{-|-}} &= \frac{\lim_{t \rightarrow \infty} p_{l+1|1}(t)}{\lim_{t \rightarrow \infty} p_{n|\lambda}(t)} \quad (\text{S4}) \\ &= \frac{\lim_{s \rightarrow 0} s \cdot \tilde{p}_{\lambda+1|1}(s)}{\lim_{s \rightarrow 0} s \cdot \tilde{p}_{n|\lambda}(s)} \quad (\text{finite value theorem}) \\ &= \frac{\lim_{s \rightarrow 0} \omega \cdot \tilde{p}_{\lambda|1}(s)}{\lim_{s \rightarrow 0} \kappa \cdot \tilde{p}_{1|\lambda}(s)} \quad (\text{by Eq. (S2)}) \\ &= \frac{\omega \cdot \langle \lambda | \lim_{s \rightarrow 0} M^{-1}(s) | 1 \rangle}{\kappa \cdot \langle 1 | \lim_{s \rightarrow 0} M^{-1}(s) | \lambda \rangle} \quad (\text{by Eq. (S3)}) \\ &= \left( \frac{\omega}{\kappa} \right)^\lambda, \quad (\text{S5}) \end{aligned}$$

where the last step follows since we have for the tridiagonal Toeplitz matrix  $M(0)$  that  $\frac{[M(0)^{-1}]_{\lambda,1}}{[M(0)^{-1}]_{1,\lambda}} = \left( \frac{\omega}{\kappa} \right)^{\lambda-1}$ .

### A. Note on the waiting time distribution

Let us denote the waiting time distribution from the current lump in direction  $u$  given that the preceding transition was in direction  $v$  ( $u, v \in \{+, -\}$ ) with  $\Psi_{u|v}(t)$ . By definition, we have the identity

$$\lim_{t \rightarrow \infty} \Psi_{u|v}(t) = \Phi_{u|v}(t). \quad (\text{S6})$$

From Eqs. (S1) together with (S2) we can determine the Laplace-transformed waiting-time distribution as

$$\tilde{\Psi}_{+|+}(s) = \tilde{p}_{l+1|1}(s) \quad (\text{S7})$$

$$= \frac{\omega}{s} \langle \lambda | M^{-1}(s) | 1 \rangle. \quad (\text{S8})$$

For instance, with  $\lambda = 3$ , we obtain

$$\tilde{\Psi}_{+|+}(s) = \frac{\omega^3}{\text{poly}(s)}, \quad (\text{S9})$$

with  $\text{poly}(s) = s(s + \kappa + \omega) ((s + \kappa)^2 + 2s\omega + \omega^2)$ , which has roots

$$s_1 = 0, \quad s_2 = -(\kappa + \omega), \quad (\text{S10})$$

$$s_3 = -(\kappa + \omega) - \sqrt{2\kappa\omega}, \quad s_4 = -(\kappa + \omega) + \sqrt{2\kappa\omega}. \quad (\text{S11})$$

Using Cauchy's residue theorem, we can invert  $\tilde{\Psi}_{+|+}(s)$  back to time domain

$$\Psi_{+|+}(t) = \omega^3 \sum_{i=1}^4 \frac{1}{\frac{d}{ds} \text{poly}(s)|_{s=s_i}} \exp(s_i \cdot t). \quad (\text{S12})$$

It only remains to plug the roots  $s_i$  in Eqs. (S10)-(S11) into Eq. (S12). The result is a tedious linear combination of four exponentials (of which one is constant). The result is  $\Psi_{+|+}(t)$  for  $\omega = 3$ ,  $\kappa = 2$  is shown in Fig. S1 (continuous blue line) along with results from simulations (orange dots). The waiting-time distribution is clearly non-exponential, directly contradicting the assumption of Markovian dynamics on the lumped state space that is made in [1] implicitly in using the Markovian dissipation estimate.

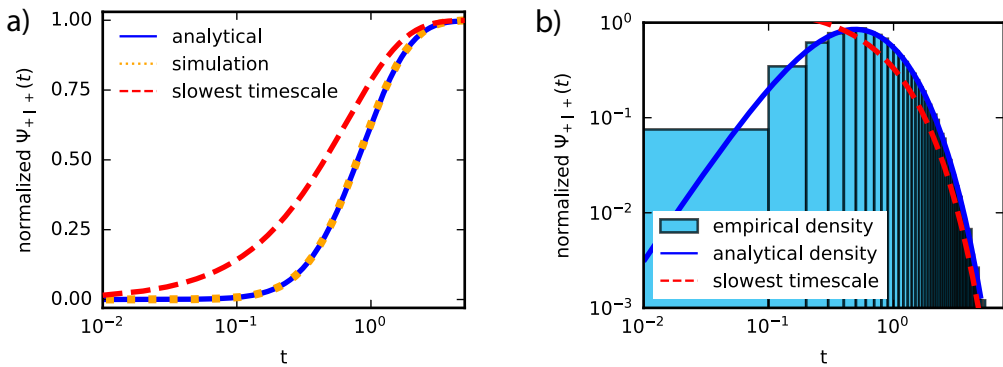


FIG. S1. Highly non-exponential waiting time density  $\Psi_{+|+}(t)$  for the lumped cycle graph with lump size  $\lambda = 3$  and parameters  $\omega = 3$ ,  $\kappa = 2$  normalized by the splitting probability: (a) Distribution functions where the analytical result (blue line) matches the simulation (dotted orange line). While the slowest timescale is exponential (red dashed line), the waiting time density is not. (b) Probability density functions in log-log scale. The exponential, slowest time scale can be seen as a cut-off (dashed red) of the non-exponential waiting time density.

For the calculation of the waiting time distribution in the reverse direction,  $\Psi_{-|-}(t)$ , we proceed analogously. In particular, we note that the polynomial is the same, hence its roots and derivative are equal, and the only difference is the prefactor

$$\Psi_{-|-}(t) = \kappa^3 \sum_{i=1}^4 \frac{1}{\frac{d}{ds} \text{poly}(s)|_{s=s_i}} \exp(s_i \cdot t). \quad (\text{S13})$$

We hence have that the conditional waiting time distribution is equal in both directions

$$\frac{\Psi_{+|+}(t)}{\Phi_{+|+}} = \frac{\Psi_{-|-}(t)}{\Phi_{-|-}}, \quad \forall t \in \mathbb{R}^+. \quad (\text{S14})$$

Thus, in particular, their Kullback-Leibler divergence vanishes  $D_{\text{KL}} \left[ \frac{\Psi_{+|+}(t)}{\Phi_{+|+}} \left\| \frac{\Psi_{-|-}(t)}{\Phi_{-|-}} \right. \right] = 0$ , so that waiting times do *not* contribute to the entropy production rate, which is in turn fully captured by the splitting probabilities [2].

### III. TREE GRAPH

We now consider the lumped tree of (edge) depth  $d$  with lumps of depth  $l$ . Let the underlying microscopic graph  $G_T$  be constructed as described in Appendix A and depicted in Fig. 1a in the Letter. The steady state is the uniform distribution as can be readily seen from the generator  $L$ .

#### A. Microscopic dynamics

The entropy production rate of the microscopic system can be computed with a cycle decomposition. Let  $T$  be the spanning tree obtained from  $G_T$  with all edges between levels  $U_d$  and  $U_0$  removed. Let  $\mathcal{C}$  be the cycle basis induced by  $T$  [3]. For any  $c \in \mathcal{C}$ , the cycle's current is determined by the flux of the chord – i.e. the edge between  $U_d$  and  $U_0$ , yielding

$$J_c = \frac{\omega - \kappa}{n2^d}, \quad (\text{S15})$$

where the factor  $n^{-1}$  stems from the steady state and is determined through depth  $d$ .

The affinity of  $c$  is

$$A_c = (d+1) \ln \left( \frac{\omega}{\kappa} \right). \quad (\text{S16})$$

Since the dimension is  $|\mathcal{C}| = 2^d$ , we get an entropy production rate

$$\dot{S} = \sum_{c \in \mathcal{C}} \dot{S}(c) = \sum_{c \in \mathcal{C}} J_c A_c = \frac{d+1}{2^{d+1}-1} (\omega - \kappa) \ln \left( \frac{\omega}{\kappa} \right), \quad (\text{S17})$$

where in the last step we used that the number of vertices is  $n(d) = 2^{d+1} - 1$ .

#### B. Mistaken dynamics

We now analyze what happens if we mistakenly assume Markov dynamics of the lumped state space with lump depth  $l$ . Since the steady-state distribution is uniform over all vertices, a lump of depth  $l$  has a steady-state probability

$$\mathbb{P}[\Delta] = (2^{l+1} - 1) \frac{1}{n}. \quad (\text{S18})$$

Suppose the triangle is rooted in level  $U_i$ . According to Eq. (4) in [1] the upwards “effective rate” from the triangle is

$$k_{\Delta_i \uparrow} = \frac{\kappa}{2^i \cdot (2^{l+1} - 1)}, \quad (\text{S19})$$

while the rate to a neighboring lump downward reads

$$k_{\Delta_i \downarrow} = \frac{\omega}{2^{i+l+1} \cdot (2^{l+1} - 1)}. \quad (\text{S20})$$

For an edge between two tree lumps rooted at levels  $U_{i-l-1}$  and  $U_i$ , we have

$$\dot{S}_{\text{single edge } \Delta_{i-l-1} \leftrightarrow \Delta_i} \quad (\text{S21})$$

$$= \mathbb{P}[\Delta] (k_{\Delta_{i-l-1} \downarrow} - k_{\Delta_i \uparrow}) \ln \left( \frac{k_{\Delta_{i-l-1} \downarrow}}{k_{\Delta_i \uparrow}} \right) \quad (\text{S22})$$

$$= \frac{1}{n2^i} (\omega - \kappa) \ln \left( \frac{\omega}{\kappa} \right). \quad (\text{S23})$$

There are  $2^i$  such edges, which contribute

$$\dot{S}_{\text{all edges on level } \Delta_{i-l-1} \leftrightarrow \Delta_i} = \frac{1}{n} (\omega - \kappa) \ln \left( \frac{\omega}{\kappa} \right). \quad (\text{S24})$$

There are  $\frac{d+1}{l+1}$  such transitions between levels, so that we get with  $n \equiv n(d) = 2^{d+1} - 1$  an entropy production rate

$$\dot{S}_M = \frac{d+1}{2^{d+1}-1} \frac{1}{l+1} (w-k) \ln\left(\frac{\omega}{\kappa}\right) \quad (\text{S25})$$

$$= \frac{d+1}{2^{d+1}-1} \frac{\ln(2)}{\ln(\lambda+1)} (w-k) \ln\left(\frac{\omega}{\kappa}\right) \propto \frac{1}{\ln(\lambda+1)}, \quad (\text{S26})$$

where in the last step we used that  $\lambda \equiv n_0/n_s = 2^{l+1} - 1$ . This result is illustrated for the case  $d = 23$  (and thus  $n = 16777215$ ) in Fig. 2b in the letter.

### C. Mesosystem

We now derive the entropy production rate of the lumped mesosystem when memory is accounted for. Via Laplace transforms, we obtain the splitting probabilities. We defer the derivation to the more general setting in Section VI. For the special setting of the tree graph, we obtain using Eq. (S50) for the ratio of splitting probabilities

$$\frac{\Phi_{+|+}}{\Phi_{-|-}} = \left(\frac{\omega}{\kappa}\right)^{l+1}. \quad (\text{S27})$$

There are  $\frac{d+1}{l+1}$  lump levels. The net flux between each level is  $J = \frac{\omega-\kappa}{n}$ , yielding a 2<sup>nd</sup> order estimate of the entropy production rate

$$\dot{S}_2^{\text{est}} = J \ln\left(\frac{\Phi_{+|+}}{\Phi_{-|-}}\right) = (d+1) \frac{\omega-\kappa}{2^{d+1}-1} \ln\left(\frac{\omega}{\kappa}\right), \quad (\text{S28})$$

which is exact by Eq. (S17).

## IV. SIERPINSKI-TYPE GRAPH

In this section, we first calculate the dissipation rate on the fractal Sierpinski-type graph of depth  $d = 3$  on each length scale and then show a comparison of the estimator for the entropy production with the analytic solution up to depth  $d = 5$  ( $n = 3072$  vertices).

### A. Decomposition in cycle basis

We decompose the Sierpinski-type graph of depth  $d = 3$  in a cycle basis. To do so, we consider the spanning tree depicted as in Fig. S2. Recall from the Letter that we have polygons driven by rate  $\omega$  at different depths: At the finest scale (depth 1 subgraphs), the triangles are driven with rate  $\omega$ . At the next scale (depth 2) the hexagons are driven by  $\omega$ . Finally, the outermost regular polygon, the nonagon (depth 3), is also driven by  $\omega$ . See Fig. 1c in the Letter for an illustration of the driving. All other edges (and the backward edges of the driven edges) have a transition rate 1.

The elements of the induced cycle basis with non-zero current are depicted in Fig. S3. These basis elements coincide with the driven cycles at depth 1 (blue), depth 2 (green), and depth 3 (orange). While the inner subgraph  $D$  at depth 2 recomposes perfectly into its driven cycles, each outer subgraph at depth 2 has in addition two corrective cycles, which will be hidden at coarse grainings of scale  $\lambda \geq 12$  (depth  $\geq 2$ ).

A driven regular cycle at depth  $l$  has an affinity of  $A_l = 3l \log \omega$ . When driven with  $\omega = 2$ , the contribution of each scale is shown in Table. I.

### B. Comparison of stochastic estimator to analytic solution

We compare the entropy production rate obtained by the stochastic estimator for the microscopic graph to the analytic entropy production rate obtained by solving for the nullspace of the estimator, at a driving of  $\omega = 2$ . Note that, remarkably, although the graph becomes very large (at depth  $d = 6$  we have  $n = 3072$  many vertices), the matrix is sparse enough to find the steady state analytically at that size. The results summarized in Table II confirm that the estimator is indeed very precise.

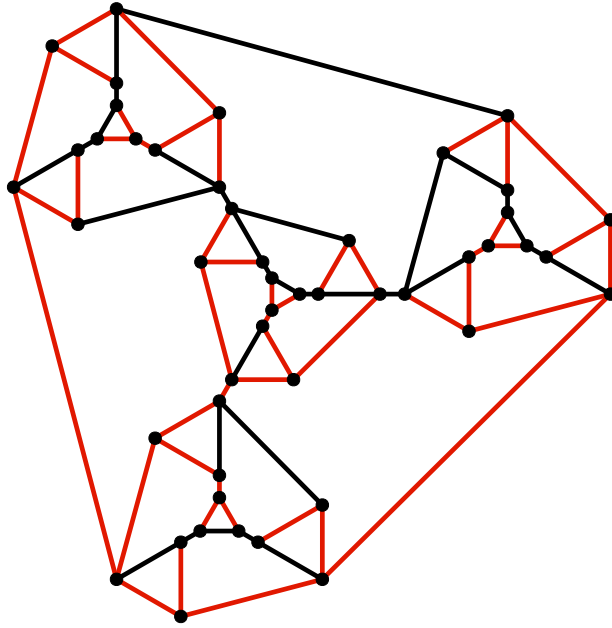


FIG. S2. Spanning tree for Sierpinski-type graph of depth  $d = 3$  inducing the considered cycle decomposition.

TABLE I. Contribution of cycle basis elements at different scales.

Basis cycles	Contribution to $\dot{S}$
Depth 1	0.59
Depth 2	0.17
Depth 3	0.07
Corrective cycles	-0.01

## V. BRUSSELATOR

For the Brusselator we choose the parameters as in [1]. Note that the state space can be reduced from  $500 \times 500$  states to e.g.  $450 \times 450$  states due to the location of the limit cycle in the steady state. This can be verified numerically, by plotting the average time spent in a given state in the steady state. We show this statistic in Fig. S4 for a trajectory of length  $5 \cdot 10^8$  after skipping an initial phase of  $10^9$  steps ensuring convergence to the steady state, where in particular the right and top region is 0 (black). Indeed, summing the steady-state probabilities for  $x > 450, y > 450$ , we get  $2.45e - 6$ .

In the Sierpinski-type graph, we were able to exploit the sparsity of the generator to find a basis for the null space. However, in the case of the Brusselator, this corresponds to finding the basis of the null space of a  $202500 \times 202500$  matrix. We are not aware of any computational solution providing reliable results without significant errors for such matrix sizes, therefore we resort to stochastic simulations.

TABLE II. Estimated entropy production rate  $\dot{S}_1^{\text{est}}$  vs. analytic solution  $\dot{S}$  for Sierpinski-type graphs of different depth. The estimation is based on trajectories of length  $10^8$  steps, after skipping  $10^8$  initial "equilibration" steps.

Depth of Sierpinski-type graph	$n$	$\dot{S}_1^{\text{est}}$	$\dot{S}$
2	12	0.8011	0.8010
3	48	0.8255	0.8259
4	192	0.8325	0.8323
5	768	0.8349	0.8341
6	3072	0.8349	0.8346

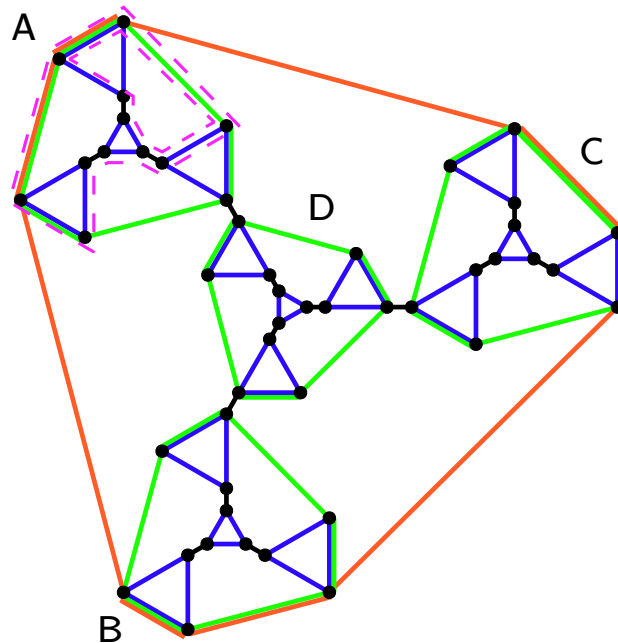


FIG. S3. Basis cycles with non-zero current. These basis elements coincide with the driven cycles of depth 1 (blue), depth 2 (green), and depth 3 (orange) as well as two corrective cycles in each of the outer subgraphs A, B, and C. These correction cycles are indicated by dashed lines in subgraphs A.

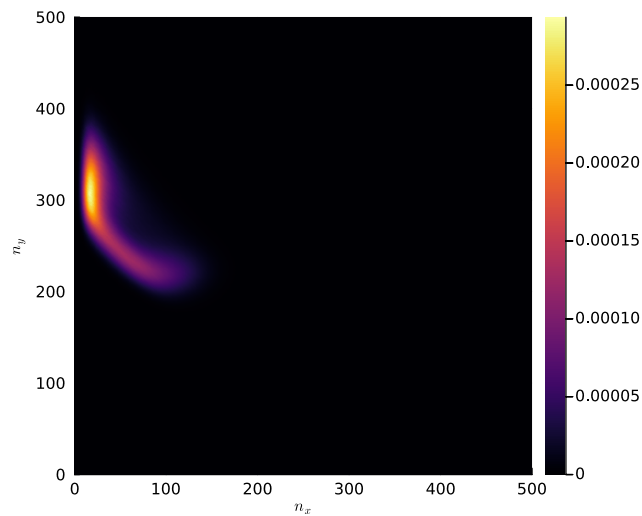


FIG. S4. Average time spent in a given state in the steady state of the Brusselator. The results were inferred from a trajectory of length  $5 * 10^8$  upon skipping  $10^9$  steps to reach the steady state.

## VI. TREE DIAMOND GRAPH

Here we consider a depth- $d$  tree diamond graph as described in Appendix C and Fig. 4a in the Letter.

## A. Construction

The tree diamond is constructed from two perfect binary trees of edge depth  $d$ , the top one rooted at the top, the bottom one rooted at the bottom, merging them to have the same set of leaves, and connecting the two roots with a bidirectional edge. Fig. 4a in the Letter shows a tree diamond of depth  $d = 5$ . Hence, the tree diamond has

$$n \equiv n(d) = 3 \cdot 2^d - 2 \quad (\text{S29})$$

vertices. In this way, we obtain edges on levels  $U_0, \dots, U_{2d}$ : Levels  $U_0, \dots, U_{d-1}$  are the levels of the upper tree, level  $U_d$  are the child nodes of both trees and levels  $U_{d+1}, \dots, U_{2d}$  are the levels of the bottom tree. Hence, the very top level  $U_0$  consists of only one vertex, as does the very bottom level  $U_{2d}$ . The rates along edges between levels of the top tree halve each step and double between levels of the bottom tree.

When walking on the tree, we go in *positive* direction, if we go from a level  $U_i$  to  $U_{i+1 \bmod 2d+1}$ . Hence, the rates of the edges between levels  $U_i$  and  $U_{i+1 \bmod 2d}$  sum to  $\omega$  in + direction and  $\kappa$  in - direction. From  $0 = Lp$  we see that the steady state is the uniform distribution over all vertices.

For any  $l \in \mathbb{N}$  with  $d+1 = 0 \bmod l+1$ , we perform a coarse-graining of depth  $l$  as follows. We start from the top root, lumping trees of depth  $l$  as we go downwards towards the leaves. We do the same from the bottom root upwards. Those up- and down-facing trees in the center, which share the same set of leaves, are merged pairwise into one lump, which is again a smaller diamond tree. A lumping of depth  $l = 1$  and  $l = 2$  is shown in Fig. 4a in the Letter in shaded blue and dashed red, respectively.

## B. Microscopic dynamics

We provide the following two different ways of estimating the *microscopic* entropy production rate  $\dot{S}$ : One via the direct formula for Markovian systems which was used by Yu et al. for *both* Markovian and non-Markovian systems. The second derivation is based on the graph decomposition in its cycle basis and hence is more instructive for the understanding of dissipative cycles.

### 1. $\dot{S}$ via edges

Let us consider an edge in the top tree, i.e. from level  $U_i$  to level  $U_{i+1}$  with  $i \in \{0, \dots, d-1\}$ . This edge contributes to the entropy production rate as

$$\dot{S}_{\text{single edge } U_i \leftrightarrow U_{i+1}} = \frac{1}{n} \frac{1}{2^{i+1}} (\omega - \kappa) \ln \left( \frac{\omega}{\kappa} \right), \quad (\text{S30})$$

where the first factor comes from the uniform steady-state probability distribution and the second from the transition rates. There are  $2^{i+1}$  such edges, so that

$$\dot{S}_{\text{level } U_i \leftrightarrow U_{i+1}} = \frac{1}{n} (\omega - \kappa) \ln \left( \frac{\omega}{\kappa} \right). \quad (\text{S31})$$

Since there are  $2d$  such levels (edges in the bottom half contribute equally by symmetry) as well as one edge connecting the bottom to the top, we have an overall entropy production rate of

$$\dot{S} = \frac{2d+1}{n(d)} (\omega - \kappa) \ln \left( \frac{\omega}{\kappa} \right), \quad (\text{S32})$$

which is stated in the Letter.

### 2. Cycle decomposition

Let our diamond tree be the graph  $G = (V, E)$ .  $G$  has a cycle basis  $\mathcal{C} = \{c_1, \dots, c_{2d}\}$  of size  $|\mathcal{C}| = 2^d$ , with each basis cycle  $c_i$  being the unique cycle of length  $2d+1$  going through a unique node in level  $L_d$ . To see this, take as spanning tree  $T$  the graph  $G$  with all edges between level  $L_d$  and  $L_{d+1}$  removed. Adding any single edge between  $L_d$  and  $L_{d+1}$  will create a cycle. We call the added edge a *chord* and identify uniquely each cycle  $c_i$  with its chord  $h_i \in E$ . Four of these cycles are highlighted at the central levels in Fig. 4a (inset) of the Letter.

We focus on a cycle  $c_i$ . This cycle's flux is determined by the flux of its chord  $h_i$ :

$$J_{c_i} = \frac{\omega - \kappa}{n2^d}, \quad (\text{S33})$$

where the factor  $n^{-1}$  stems from the steady state and  $2^{-d}$  from the transition rates. The affinity of  $c_i$  is

$$A_{c_i} = (2d + 1) \ln \left( \frac{\omega}{\kappa} \right), \quad (\text{S34})$$

since the cycle has length  $|c_i| = 2d + 1$ . Thus, the cycle's entropy production rate is [3]

$$\dot{S}_{c_i} = J_{c_i} \cdot A_{c_i} = \frac{2d + 1}{n2^d} (\omega - \kappa) \ln \left( \frac{\omega}{\kappa} \right). \quad (\text{S35})$$

Since there are  $2^d$  basis cycles, we have an overall entropy production rate of

$$\dot{S} = \sum_{c_i} J_{c_i} \cdot A_{c_i} = \frac{2d + 1}{n(d)} (\omega - \kappa) \ln \left( \frac{\omega}{\kappa} \right), \quad (\text{S36})$$

where we indicated with  $n(d)$  that  $n$  is determined by  $d$ , cf. Eq. (S29).

### C. Mesosystem

We now consider a coarse-graining of the tree diamond graph yielding a 2<sup>nd</sup>-order semi-Markov process. Hence, we need to condition the previous, current, and next mesoscopic states to have fully defined waiting times. We hence introduce  $\Psi_{x|u,y}(t)$  for  $x, y \in \{+, -\}$ ,  $u \in V$  as the distribution of transitioning from  $u$  in  $x$  direction by time  $t$  given that we transitioned to  $u$  in  $y$  direction at time  $t = 0$ . The splitting probability is the then limit  $\Phi_{x|u,y} \equiv \lim_{t \rightarrow \infty} \Psi_{x|u,y}(t)$ .

We now determine  $\Phi_{+|u,+}$ ,  $\Phi_{-|u,-}$  for  $u$  being the entry/exit point of both (a) tree and (b) tree-diamond lumps.

#### 1. Splitting probability $\Phi$ for tree lump

Consider a tree of (edge) depth  $l$ , which is w.l.o.g. rooted at its top vertex. We label the vertex levels *within that tree* by  $W_i$ ,  $i \in \{0, \dots, l\}$  so that level  $W_i$  has  $|W_i| = 2^i$  vertices. By symmetry, it suffices to consider  $P_{W_i}(t)$ , the probability of being in *any* of the vertices of level  $W_i$ . Let  $(\lambda\omega, \lambda\kappa)$  for  $\lambda \in \{2^{-k} \mid k \in \mathbb{N}_0\}$  be the weight of the edge entering the tree's root (i.e.  $W_0$ ) from above. The choice of  $k$  depends on the level  $U_j$  of the diamond tree in which the considered tree is rooted.

We can describe the evolution by the following system of ordinary differential equations. For  $i \in \{1, \dots, l - 1\}$ , we have

$$\frac{dP_{W_i}(t)}{dt} = \lambda (\omega P_{W_{i-1}}(t) + \kappa P_{W_{i+1}}(t) - (\kappa + \omega) P_{W_i}(t)), \quad (\text{S37})$$

whereas for the boundaries  $i \in \{0, l\}$ , we have

$$\frac{dP_{W_0}(t)}{dt} = \lambda (\kappa P_{W_1}(t) - (\kappa + \omega) P_{W_0}(t)) \quad (\text{S38})$$

$$\frac{dP_{W_l}(t)}{dt} = \lambda (\omega P_{W_{l-1}}(t) - (\kappa + \omega) P_{W_l}(t)). \quad (\text{S39})$$

Since we consider first-passage times, we place an absorbing state  $S$  at the lower-labeled end, and an absorbing state  $D$  at the higher-labeled end with

$$\frac{dP_S(t)}{dt} = \lambda \kappa P_{W_0}(t) \quad (\text{S40})$$

$$\frac{dP_D(t)}{dt} = \lambda \omega P_{W_l}(t). \quad (\text{S41})$$



Since these two states do *not* influence the probability distribution of the non-absorbing states, we first solve the system of non-absorbing states and then for the absorbing states. The initial distribution is either  $\mathbf{1}_{W_0}$  (in the + | + setting) or  $\mathbf{1}_{W_l}$  (in the - | - setting).

To solve the system of  $l + 1$  differential equations, we Laplace transform ( $\tilde{P}_{W_i}(s) \equiv \int_0^\infty P_{W_i}(t) \exp(-st) dt$ ). Solving for the Laplace-transformed distributions reduces to solving the following tridiagonal linear system of equations

$$\begin{pmatrix} s + \lambda k + \lambda w & -\lambda k & & & \\ -\lambda w & s + \lambda k + \lambda w & -\lambda k & & \\ & \ddots & \ddots & \ddots & \\ & & -\lambda w & s + \lambda k + \lambda w & -\lambda k \\ & & & -\lambda w & s + \lambda k + \lambda w \end{pmatrix} \begin{pmatrix} \tilde{P}_{W_0}(s) \\ \vdots \\ \tilde{P}_{W_l}(s) \end{pmatrix} = \begin{pmatrix} a \\ 0 \\ \vdots \\ 0 \\ 1 - a \end{pmatrix}, \quad (\text{S42})$$

where  $a \equiv 1$  iff we start at the root (in the + | + setting) and  $a \equiv 0$  else (in the - | - setting).

For any  $l$ , we can solve the above equation to obtain  $\tilde{P}_{W_i}(s)$  explicitly. It remains to perform an inverse Laplace transform, for which we use Cauchy's residue method. We show the result here for  $l = 2$  in the + | + setting, the "program" being analogous for every other value of  $l \in \mathbb{N}$  and directional conditions. Solving Eq. (S42) yields

$$\tilde{P}_{W_2}(s) = \frac{\lambda^2 \omega^2}{(s + \lambda \kappa + \lambda \omega) [(s + \lambda \kappa + \lambda \omega)^2 - 2\kappa \lambda^2 \omega]}. \quad (\text{S43})$$

The roots of the denominator are

$$s_1 \equiv -\lambda(\kappa + \omega) \quad (\text{S44})$$

$$s_{2/3} \equiv -\lambda(\kappa + \omega) \pm \lambda \sqrt{2\kappa \omega}, \quad (\text{S45})$$

yielding residue values of  $-\frac{\omega}{2\kappa}, \frac{\omega}{4\kappa}, \frac{\omega}{4\kappa}$  (the first derivative of the denominator is non-zero for all of  $s_1, s_2, s_3$ ). Thus

$$P_{W_2}(t) = \frac{\omega}{2\kappa} \left\{ -\exp[-\lambda(\kappa + \omega)t] + \frac{1}{2} \exp[-\lambda(\kappa + \omega)t - \lambda \sqrt{2\kappa \omega} t] + \frac{1}{2} \exp[-\lambda(\kappa + \omega)t + \lambda \sqrt{2\kappa \omega} t] \right\}, \quad (\text{S46})$$

and hence by Eq. (S41)

$$P_{W_D}(t) = \frac{\lambda \omega^2}{2\kappa} \left\{ -\exp[-\lambda(\kappa + \omega)t] + \frac{1}{2} \exp[-\lambda(\kappa + \omega)t - \lambda \sqrt{2\kappa \omega} t] + \frac{1}{2} \exp[-\lambda(\kappa + \omega)t + \lambda \sqrt{2\kappa \omega} t] \right\}. \quad (\text{S47})$$

As we argued before, this first-passage time corresponds to the distribution of transitioning in a positive direction, given that we transitioned at time  $t = 0$  in a positive direction to a tree lump. More precisely, this means for  $\Delta$  being a tree mesoscopic state rooted at its lowest microstate

$$\Psi_{+|\Delta,+}(t) = P_{W_D}(t) = \frac{\lambda \omega^2}{2\kappa} \left\{ -\exp[-\lambda(\kappa + \omega)t] + \frac{1}{2} \exp[-\lambda(\kappa + \omega)t - \lambda \sqrt{2\kappa \omega} t] + \frac{1}{2} \exp[-\lambda(\kappa + \omega)t + \lambda \sqrt{2\kappa \omega} t] \right\}. \quad (\text{S48})$$

We may proceed analogously with the initial condition  $a = 1$  to obtain a solution for  $P_{W_0}(t)$  and

$$\Psi_{-|\Delta,-}(t) = \frac{\lambda \kappa^2}{2\omega} \left\{ -\exp[-\lambda(\kappa + \omega)t] + \frac{1}{2} \exp[-\lambda(\kappa + \omega)t - \lambda \sqrt{2\kappa \omega} t] + \frac{1}{2} \exp[-\lambda(\kappa + \omega)t + \lambda \sqrt{2\kappa \omega} t] \right\}. \quad (\text{S49})$$

since the roots  $s_i$  have the same values as in the positive direction case [4]. Note that  $s_i < 0$  for all  $\lambda, \kappa, \omega > 0, i \in [3]$ , so that the distributions indeed converge for  $t \rightarrow \infty$ .

In the exemplary case above, we chose  $l = 2$ . For general  $l$ , the ratio of splitting probabilities yields

$$\frac{\Phi_{+|\Delta,+}}{\Phi_{-|\Delta,-}} = \frac{\lim_{t \rightarrow \infty} \Psi_{+|\Delta,+}(t)}{\lim_{t \rightarrow \infty} \Psi_{-|\Delta,-}(t)} = \left(\frac{\omega}{\kappa}\right)^{l+1}. \quad (\text{S50})$$

For a triangle rooted at its highest-labelled microstate ( $\nabla$ ), we obtain by symmetry

$$\frac{\Phi_{+|\nabla,+}}{\Phi_{-|\nabla,-}} = \frac{\lim_{t \rightarrow \infty} \Psi_{+|\nabla,+}(t)}{\lim_{t \rightarrow \infty} \Psi_{-|\nabla,-}(t)} = \left(\frac{\kappa}{\omega}\right)^{-(l+1)} = \frac{\Phi_{+|\Delta,+}}{\Phi_{-|\Delta,-}}. \quad (\text{S51})$$

We corroborate the analytical results with computer experiments in Fig. S5, and find that they are in excellent agreement.

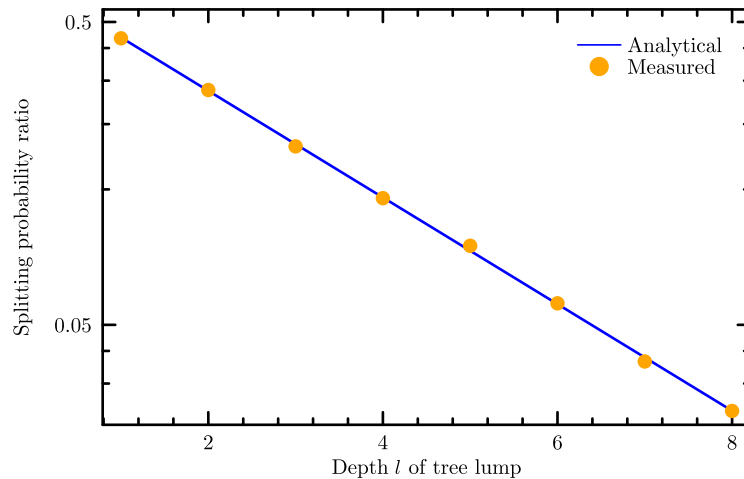


FIG. S5. Splitting probability ratio for the tree lumps of depth  $l \in [9]$  on a lin-log plot, tested here with  $\omega = 2$ ,  $\kappa = 3$ . We see that our results match with the experiments. Experiments were performed with trajectories of length  $10^5$  states per tree size.

## 2. Splitting probability $\Phi$ for tree diamond lump

We say that a tree diamond has depth  $l$  if both its top and bottom tree have (edge-) depth  $l$ . Analogously to the tree lump case, we obtain for the ratio of splitting probabilities

$$\frac{\Phi_{+|\diamond,+}}{\Phi_{-|\diamond,-}} = \left(\frac{\omega}{\kappa}\right)^{2l+1}, \quad (\text{S52})$$

which we compare in Fig. S6 to simulation results.

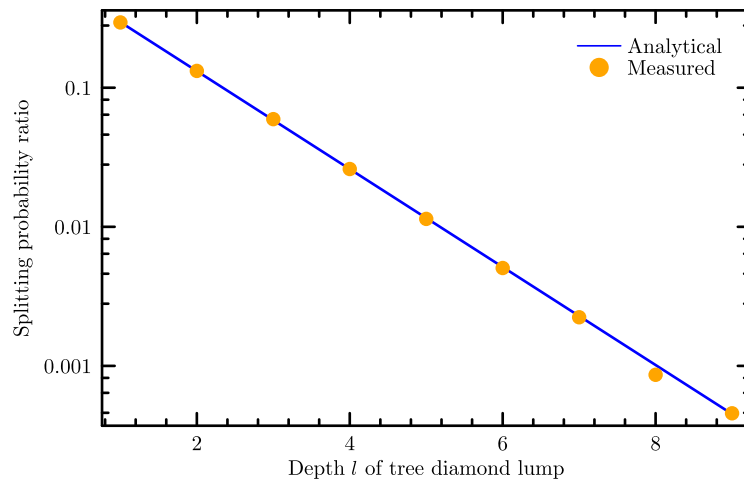


FIG. S6. Splitting probability ratio for the tree diamond lump of depth  $l \in [9]$  in a lin-log plot, tested here with  $\omega = 2$ ,  $\kappa = 3$ . The analytical results agree fully with computer experiments, which were performed with trajectories of length  $5 \times 10^5$  states per tree diamond size.

Performing a lumping of depth  $l$ , we have  $\frac{d-l}{l+1}$  many top-up triangle ( $\triangle$ ) levels, one tree diamond ( $\diamond$ ) level, and  $\frac{d-l}{l+1}$  many bottom-up triangle ( $\nabla$ ) levels. If we group each level together and describe with  $J = \frac{\omega-\kappa}{n}$  the net flux between

each level (which is constant across levels), we have the entropy production rate

$$J^{-1}\dot{S}_2^{\text{est}} = \frac{d-l}{l+1} \ln \left( \frac{\Phi_{+|\Delta,+}}{\Phi_{-|\Delta,-}} \right) + \frac{d-l}{l+1} \ln \left( \frac{\Phi_{+|\nabla,+}}{\Phi_{-|\nabla,-}} \right) + \ln \left( \frac{\Phi_{+|\diamond,+}}{\Phi_{-|\diamond,-}} \right) \quad (\text{S53})$$

$$= \frac{d-l}{l+1} \ln \left( \left( \frac{\omega}{\kappa} \right)^{l+1} \right) + \frac{d-l}{l+1} \ln \left( \left( \frac{\kappa}{\omega} \right)^{-(l+1)} \right) + \ln \left( \left( \frac{\omega}{\kappa} \right)^{2l+1} \right) \quad (\text{S54})$$

$$= (2d+1) \ln \left( \frac{\omega}{\kappa} \right), \quad (\text{S55})$$

which is exactly the microscopic entropy production rate, cf. Eq. (S32).

#### D. Average lump size

To get the average lump size, i.e. the average number of vertices per lump, for a given tree diamond graph of depth  $d$  with lump depth  $l$ , we first find the number of tree diamond lumps and tree lumps. For the former, we note that every diamond lump is rooted at level  $d-l$ , hence the number of tree diamond lumps is

$$n_{\diamond} = 2^{d-l}. \quad (\text{S56})$$

For the latter, we observe that  $2(2^{d-l}-1)$  many vertices belong to tree lumps, of which each has a size of  $2^{l+1}-1$ , yielding

$$n_{\Delta} = \frac{2(2^{d-l}-1)}{2^{l+1}-1} \quad (\text{S57})$$

many triangle lumps. Thus, the average size per lump is

$$\lambda_{l,d} = \frac{n_{\text{vtcs}}}{n_{\diamond} + n_{\Delta}} = \frac{(2^{l+1}-1)(3 \cdot 2^d - 2)}{2(2^d - 1 + 2^{d-l-1})} \stackrel{d \gg l \gg 1}{\approx} 3 \cdot 2^l. \quad (\text{S58})$$

#### E. Mistaken dynamics

We now explore what happens if the mesoscopic dynamics are *mistakenly* assumed to be Markovian with effective rates. As before, we enumerate the vertex levels of the tree diamond graph by  $0, \dots, 2d$ .

Since the steady-state distribution is uniform over all vertices, a lumped tree of depth  $l$  has probability

$$\mathbb{P}[\Delta] = (2^{l+1}-1) \frac{1}{n}. \quad (\text{S59})$$

Suppose the triangle is rooted in level  $U_i$ , with w.l.o.g  $i \in \{0, \dots, d-2l-1\}$  [5]. The rate from the triangle upwards, following Eq. (4) in [1], is

$$k_{\Delta_i \uparrow} = \frac{\kappa}{2^i \cdot (2^{l+1}-1)}, \quad (\text{S60})$$

and the rate to a single lump downward is

$$k_{\Delta_i \downarrow} = \frac{\omega}{2^{i+l+1} \cdot (2^{l+1}-1)}. \quad (\text{S61})$$

For  $i \in \{l+1, \dots, d-2l-1\}$  and an edge between two tree lumps rooted at levels  $U_{i-l-1}$  and  $U_i$ , we have

$$\dot{S}_{\text{single edge } \Delta_{i-l-1} \leftrightarrow \Delta_i} \quad (\text{S62})$$

$$= \mathbb{P}[\Delta] (k_{\Delta_{i-l-1} \downarrow} - k_{\Delta_i \uparrow}) \ln \left( \frac{k_{\Delta_{i-l-1} \downarrow}}{k_{\Delta_i \uparrow}} \right) \quad (\text{S63})$$

$$= \frac{1}{n2^i} (\omega - \kappa) \ln \left( \frac{\omega}{\kappa} \right). \quad (\text{S64})$$

There are  $2^i$  such edges, such that we have

$$\dot{S}_{\text{all edges on level } \Delta_{i-l-1} \leftrightarrow \Delta_i} = \frac{1}{n} (\omega - \kappa) \ln \left( \frac{\omega}{\kappa} \right). \quad (\text{S65})$$

For a tree diamond lump of depth  $l$ , we have analogously

$$\mathbb{P}[\diamond] = (3 \cdot 2^l - 2) \frac{1}{n}, \quad (\text{S66})$$

with rates for a tree diamond lump rooted at level  $i = d - l$  according to [1]

$$k_{\diamond_i \uparrow} = \frac{\kappa}{2^i \cdot (3 \cdot 2^l - 2)} \quad (\text{S67})$$

$$k_{\diamond_i \downarrow} = \frac{\omega}{2^i \cdot (3 \cdot 2^l - 2)}. \quad (\text{S68})$$

Thus, for all edges from the triangles to diamonds in the upper half, we have

$$\dot{S}_{\text{all edges on level } \Delta_{d-2l-1} \leftrightarrow \diamond_{d-l}} = \frac{1}{n} (\omega - \kappa) \ln \left( \frac{\omega (3 \cdot 2^l - 2)}{\kappa (2^{l+1} - 1)} \right), \quad (\text{S69})$$

$$\dot{S}_{\text{all edges on level } \diamond_{d-l} \Delta_{d+l+1} \leftrightarrow} = \frac{1}{n} (\omega - \kappa) \ln \left( \frac{\omega (2^{l+1} - 1)}{\kappa (3 \cdot 2^l - 2)} \right). \quad (\text{S70})$$

Finally, for the single edge connecting to the next macroscopic diamond tree, we have

$$\dot{S}_{\text{macroscopic edge}} = \frac{1}{n} (\omega - \kappa) \ln \left( \frac{\omega}{\kappa} \right). \quad (\text{S71})$$

We have  $2 \cdot \frac{d-l}{l+1} - 2$  many edge-levels between triangle levels, 2 edge-levels between triangles and tree-diamond lumps, and one macroscopic edge, leading to an overall *mistaken entropy production rate*

$$\dot{S}_M = \frac{1}{n(d)} (\omega - \kappa) \left( 2 \cdot \frac{d-l}{l+1} + 1 \right) \ln \left( \frac{\omega}{\kappa} \right) \neq \dot{S} = \dot{S}_2^{\text{est}}, \quad (\text{S72})$$

which is reported in the Letter.

## VII. TECHNICALITIES OF THE SAMPLING PROCEDURE

### A. Exploiting the symmetry of the graph

In the cases of the tree graph and tree diamond graph, we use the graph symmetry to increase the statistical precision: all lumps on a given level have (1) equal steady state probability, (2) equal transition rates, predecessors, and successors (important for the memory of the stochastic process), and (3) no edge connects them. Thus, after simulating the microscopic dynamics, we may in the statistical analysis w.l.o.g. treat all lumps on a given level as equal, which increases the statistics per lump. Note that this is are very particular properties of the problems' symmetry and may *not* be used in general, e.g. not for the Brusselator.

### B. Choice of parameters

For the results shown in the Letter, we chose  $w = 2$ ,  $\kappa = 1$  for both the ring and tree graph. For the tree diamond graph, we chose  $w = 2$ ,  $\kappa = 3$ .

For the Sierpinski-type graph (Fig. 3a in the Letter), trajectories were drawn after  $N_{\text{skip}} = 10^9$  initial steps and are of length  $N_{\text{steps}} = 5 \times 10^8$ . The plot shows the average of 108 trajectories, with almost vanishing error bars. We took  $w = 2$  for the driving.

For the Brusselator, (Fig. 3b in the Letter), trajectories were drawn after  $N_{\text{skip}} = 10^9$  initial steps and are of length  $N_{\text{steps}} = 10^9$ . The plot shows the average of 25 trajectories with almost vanishing error bars. We note that the state

space is very large with many states having steady-state probability almost 0 but non-vanishing transition rates. In the microscopic setting,  $\lambda = 1$ , this may lead to undersampling of the steady state. Similarly, order  $k \geq 4$  would need even longer trajectories.

In all cases, the fitted lines were least-squares-fitted to the measurements on all scales except for the smallest and largest scale [1], which clearly deviate in the tree, diamond tree, Sierpinski-type graph, and Brusselator, i.e. where we do *not* have a power law of the entropy production rate in the scale.

### C. Subsampling for higher orders

For higher-order estimators, we need exponentially longer trajectories, since statistics of tuples of length  $k + 1$  for order  $k$  estimators need to be drawn and sampled sufficiently. We see in Fig. S7a that the order  $k = 4$  estimator struggles for the coarsest scales, however *not* due to high fluctuations among the 100 trajectory measurements, but instead as a systematic under-sampling error. For 5 times longer trajectories (Fig. S7b) we see significant enhancement on the second coarsest scale. Increasing the trajectory length by a factor of 10 (Fig. S7c) does not yield significant improvement, underlining the non-linear requirement of sample statistics in the order  $k$ .

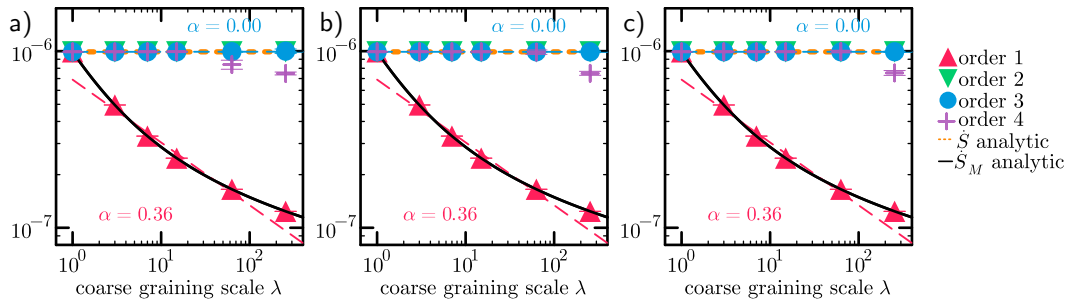


FIG. S7. Entropy production rate on the tree graph as a function of the coarse-graining scale for different sample path lengths: (a) For paths of length  $10^8$  (b) of length  $5 \cdot 10^8$  (c) of length  $10^9$ . All trajectories were recorded after initial  $N_{\text{skip}} = 10^8$  many steps. Depicted are averages of 100 such trajectories with standard deviation indicated through the error bars.

- 
- [1] Q. Yu, D. Zhang, and Y. Tu, Inverse Power Law Scaling of Energy Dissipation Rate in Nonequilibrium Reaction Networks, *Phys. Rev. Lett.* **126**, 080601 (2021).
  - [2] I. A. Martínez, G. Bisker, J. M. Horowitz, and J. M. R. Parrondo, Inferring broken detailed balance in the absence of observable currents, *Nat Commun* **10**, 3542 (2019).
  - [3] J. Schnakenberg, Network theory of microscopic and macroscopic behavior of master equation systems, *Rev. Mod. Phys.* **48**, 571 (1976).
  - [4] Even stronger, inverting the matrix from Eq. (S42) yields the same denominator for each entry, hence we get the same roots, and hence the same powers of the exponentials in the waiting time distribution.
  - [5] The last level in the upper half of the macroscopic tree diamond that roots a tree lump is level  $d - 2l - 1$ .